Bulletin of Mathematical Biology manuscript No.
(will be inserted by the editor)

Modeling the role of feedback in the adaptive response of bacterial quorum sensing.

Gaoyang Fan[1] **and Paul C. Bressloff**[1]

Department of Mathematics, University of Utah, Salt Lake City, UT 84112 USA

The date of receipt and acceptance will be inserted by the editor

Abstract Bacterial quorum sensing (QS) is a form of intercellular communication that relies on the production and detection of diffusive signaling molecules called auotinducers. Such a mechanism allows the bacteria to track their cell density in order to regulate group behavior, such as biofilm formation and bioluminescence. In a number of bacterial QS systems, including *V. harveyi*, multiple signaling pathways are integrated into a single phosphorylation-dephosphorylation cycle. In this paper, we propose a weight control mechanism, in which QS uses feedback loops to 'decode' the integrated signals by actively changing the sensitivity in different pathways. We first use a slow/fast analysis to reduce a single cell model to a planar dynamical system involving the concentrations of phosphorylated signaling protein LuxU and a small non-coding RNA. In addition to identifying the weight control mechanism, we show that adding a feedback loop can lead to a bistable QS response in certain parameter regimes. We then combine the slow/fast analysis with a contraction mapping theorem in order to reduce a population model to an effective single-cell model, and show how the weight control mechanism allows bacteria to have a finer discrimination of their social and physical environment.

1 Introduction

Quorum sensing (QS) is a form of cell-cell communication that allows bacteria to measure the local population density, and to use this as a cue to regulate gene expression, resulting in various forms of collective bacterial response, including bioluminescence, biofilm formation and virulence [6,3, 4,15,26,10,19,18,29,20]. Bacterial QS depends on the production, secretion and detection of signaling molecules known as autoinducers (AIs). In particular, high population densities lead to high intracellular AI concentrations through diffusive exchange with the extracellular environment, triggering biochemical reactions that activate the expression of QS-controlled genes. One can view the QS system as a 'switch' controlling the level of downstream gene expression. In some cases the QS system acts as a 'toggle' or binary switch [32], such that the QS-regulated genes are only expressed in the 'ON' state. In other cases, QS-regulated genes are expressed in a graded fashion [17], and the QS system acts like a 'dimmer' switch. In this paper we will associate 'OFF' and 'ON' states with low and high levels of QS-regulated gene expression.

In the case of the bacterium *V. harveyi*, three different kinds of AI have been identified, which encode different types of population information: HAI-1 (an intra-species signal), CAI-1 (an intra-genera signal) and AI-2 (the universal signal) [27]. Each autoinducer is detected by its corresponding cognate receptor, LuxN, CqsS, and LuxPQ, respectively, and integrated into the phosphorylation-dephosphorylation cycle (PdPC) of a downstream protein LuxU. At low cell density, in the absence of AI, an unbound receptor functions as a kinase and phosphorylates the protein LuxU. This leads to the phosphorylation of a second protein LuxO and subsequent activation of small non-coding RNAs (sRNAs) known as qrr 1-5. The latter repress the translation of the mRNA that encodes the master quorum-sensing regulator LuxR, which turns QS 'OFF'. On the other hand, at high cell density, AI binds to its receptor, switching the action of the latter to a phosphatase, which in turn, drains the phosphate group from LuxO and LuxU. This results in the deactivation of the sRNAs and the production of LuxR, which turns QS 'ON'.

Recently, we developed a feedforward population model of QS in *V. harveyi* [1,5]. The model consists of a system of ordinary differential equations (ODEs) that represent the interchange of AI between the cytoplasm of N cells and an extracellular domain, and the binding of intracellular AI to cognate receptors within each cell. The unbound and bound receptors are treated as kinases and phosphatases, respectively, acting on a single downstream PdPC network. For simplicity, the model ignores subsequent signaling pathways associated with gene regulation and the possible modification in the production rate of AI (positive or negative feedback). We used the model to explore the signal integration of multiple parallel input pathways, representing different kinds of AI acting on the same downstream PdPC. In particular, we investigated to what extent a pair of pathways

could distinguish between two environmental cues: cell density and mass transfer in the case of a single bacterial population, and the cell densities of two distinct bacterial populations. We showed that the additive nature of signal integration limited the degree to which different environmental cues could be distinguished. In this paper, we extend our previous study of signal integration in *V. harveyi* QS by including the effects of feedback.

Biological Motivation. Experimentally, it has been shown that there are at least five feedback loops in *V. harveyi* quorum sensing circuits [27,28], see Fig.1. These can be partitioned into a *qrr*-LuxO-LuxU component, a *qrr*-LuxR component, and a third component involving *qrr* 1-4 repressing the production of receptor LuxN. Experimental data suggests that the role of the LuxN feedback loop is to adjust the relative sensitivity to AI signals from a low cell density environment to a high cell density environment [27], whereas the other feedback loops control the dynamic range of responses. The roles of both LuxO and LuxR feedback loops have been studied in Ref. [13]. (However, these authors focus on the qss signaling network and do not explicitly model the PdPC.) Here we will focus on the LuxN feedback loop. Through mathematical modeling, we demonstrate the same active control of AI sensitivity due to the presence of LuxN feedback loop as observed experimentally [27]. We also highlight how the LuxN feedback loop can support a bistable response. Although the latter has not yet been observed in *V. harveyi*, or in *V. cholerae* which is another bacterium with multiple parallel QS pathways [14], *in vivo* bistability has been observed in *V. fischeri* [31,11].

The structure of the paper is as follows. In section 2, we construct a single-cell model of the QS circuit with a LuxN feedback loop, and test its response to different combinations of AI concentrations. We use mathematical modeling to identify a possible mechanism for how QS could utilize the LuxN loop to actively change the weight of different signals during the integration into the PdPC. In section 3, we apply system reduction techniques, based on a contraction mapping theorem [16,24], to reduce a population model with feedback to an effective single-cell model. In sections 4 and 5, we apply our analysis to a population-mass-transfer model and a two-population model in order to test two different hypothesis regarding the functionality of multiple parallel pathway bacteria QS: diffusion sensing (DS) and bacteria species differentiation. We combine our analysis of the population model with the weight control scheme to show how bacteria utilize the LuxN feedback loop to enhance recognition of their physical environment (mass transfer) and their social environment (bacteria species).

One final note is in order. The single cell model presented in this paper has many parameters, many of which are currently not known. Therefore, we will proceed by non-dimensionalizing the model and constructing a reduced set of lumped parameters. We then explore the qualitative behavior of the model as a function of these lumped parameters, which allows us to isolate the effects of feedback.

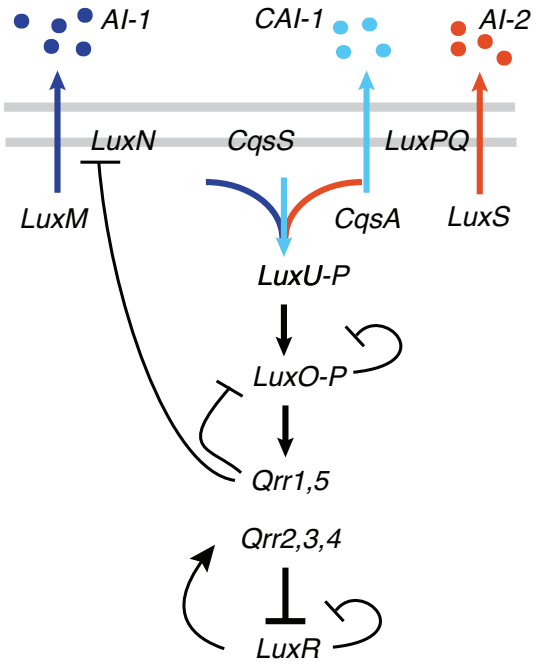


Fig. 1 Schematic diagram of feedback loops that are currently known in *V. harveyi* QS. The cognate receptors of the autoinducers AI-1, CAI-1 and AI-2 are LuxN, CqsS and LuxPQ, respectively. The arrows feeding into LuxU represent the kinase action of the receptorsThe corresponding regulators of the three autoinducers are LuxM, CqsA and LuxS. In this paper we focus on the LuxN feedback loop.

2 Single Cell Model

The single-cell version of our previous model [1,5] described the signal integration component of QS, where the PdPC of protein LuxU is driven by multiple parallel pathways. In this section, we extend the model by adding the phosphorylation and dephosphorylation of the regulator protein LuxO, the activation of qrr sRNAs, and the LuxN feedback loop. We consider M species of AI, denoted by A_i, $i = 1, \ldots, M$. The basic reaction network is shown in Fig. 2 for the ith species. The unbound and bound receptor states are denoted by R_i and $\widehat{R}_i$, respectively, with $R_{Ti} = R_i + \widehat{R}_i$. In contrast to our previous model, the total number of receptors R_{Ti} can change due to repression of the mRNA M_i that is responsible for synthesizing the receptor.

2.1 Phosphorylation-dephosphorylation cycle kinetics: no feedback

We begin by considering the PdPC circuit without feedback, which is a slightly modified version of the model considered in Ref. [5], since it also

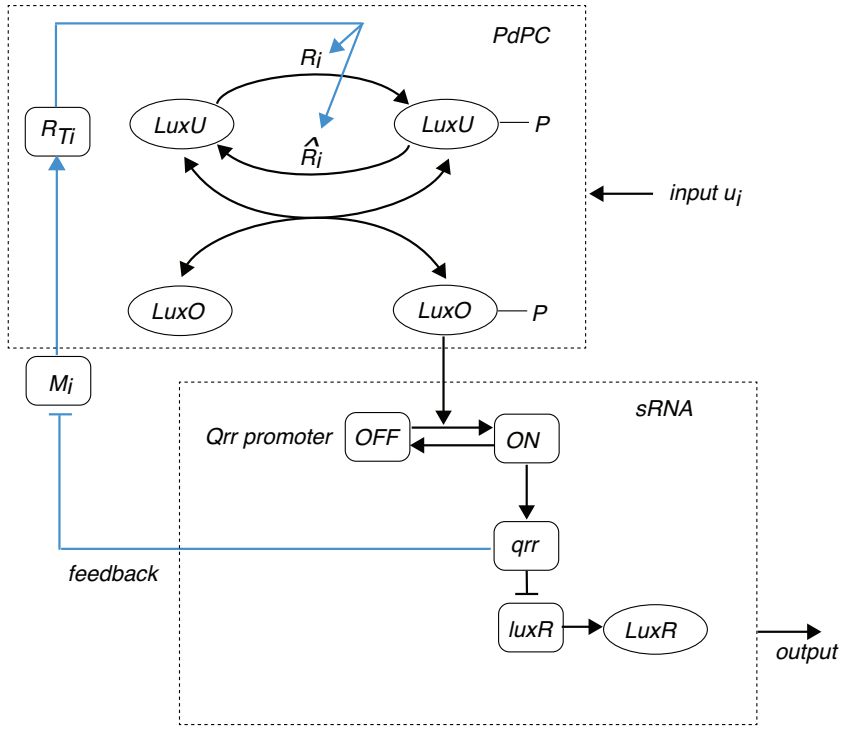


Fig. 2 Schematic representation of the LuxN feedback single cell model in *V. harveyi*. A set of autoinducers (input concentrations u_i) drive the phoshporylation-dephosphorylation cycle (PdPC) by binding to the kinase receptors R_i and converting them to phosphatases $\widehat{R}_i$. The output of the PdPC is LuxO-P, which acts as the input to the sRNA circuit. (For simplicity, we do not distinguish between the different classes of Qrr.) Activation of Qrr represses production of LuxR, which is itself the activator of downstream QS genes. Qrr also represses the production of the total number of receptors R_{Ti}, which is the source of feedback from the sRNA circuit to the PdPC circuit (indicated in blue).

includes the phosphorylation and dephosphorylation of the regulator protein LuxO. Let W represent protein LuxU and W^* represent LuxU-P. Similarly, let O represent protein LuxO and O^* represent LuxO-P. Adopting the Goldbeter-Koshland model of PdPCs [8,7,22], the PdPC with $i = 1, \ldots, M$

pathways can be represented by the following reaction scheme:

$$R_i + A_i \underset{k_{-i}}{\overset{k_i}{\rightleftharpoons}} \widehat{R}_i, \tag{2.1a}$$

$$W + R_i \underset{d_i}{\overset{a_i}{\rightleftharpoons}} WR_i \xrightarrow{g_i} W^* + R_i, \tag{2.1b}$$

$$W^* + \widehat{R}_i \underset{c_i}{\overset{b_i}{\rightleftharpoons}} W^*\widehat{R}_i \xrightarrow{h_i} W + \widehat{R}_i, \tag{2.1c}$$

$$O + W^* \underset{e_-}{\overset{e_+}{\rightleftharpoons}} OW^* \xrightarrow{e} O^* + W, \tag{2.1d}$$

$$O^* + W \underset{f_-}{\overset{f_+}{\rightleftharpoons}} O^*W \xrightarrow{f} O + W^*, \tag{2.1e}$$

The first three equations represent the contribution of the ith input pathway to the PdPC of LuxU. It is important to note that in the single-cell model the concentration of A_i is an input variable that can be directly controlled. On the other hand, in the population model analyzed in section 3, the concentration is determined self-consistently and depends on environmental states that act as the model inputs. Equations (2.1d-e) represent the phosphorylation/dephosphorylation of LuxO.

Let $[W] = w$, $[W^*] = w^*$, $[WR_i] = v_i$, $[W^*\widehat{R}_i] = v_i^*$, $[R_i] = r_i - v_i$, $[\widehat{R}_i] = \widehat{r}_i - v_i^*$, $[A_i] = u_i$, $[O] = o$, $[O^*] = o^*$, $[OW^*] = x$, $[O^*W] = y$. (Although the receptors are membrane-bound, we take all concentrations to be number of molecules per unit cell volume.) By the law of mass action, the kinetic equations for the PdPC circuit driven by fixed intracellular concentration of inducers u_i are as follows:

$$\dot{r}_i = k_{-i}\widehat{r}_i - k_i r_i u_i, \tag{2.2a}$$

$$\dot{v}_i = a_i(r_i - v_i)w - (d_i + g_i)v_i, \tag{2.2b}$$

$$\dot{v}_i^* = b_i(\widehat{r}_i - v_i^*)w^* - (c_i + h_i)v_i^*, \tag{2.2c}$$

$$\begin{aligned}\dot{w} = &\sum_{i=1}^{M}\big[- a_i(r_i - v_i)w + d_i v_i + h_i v_i^*\big] \\ &- f_+ o^* w + f_- y + ex,\end{aligned} \tag{2.2d}$$

$$\begin{aligned}\dot{w}^* = &\sum_{i=1}^{M}\big[- b_i(\widehat{r}_i - v_i^*)w^* + c_i v_i^* + g_i v_i\big] \\ &- e_+ o w^* + e_- x + fy,\end{aligned} \tag{2.2e}$$

for the PdPC of LuxU and its interactions with LuxO,

$$\dot{x} = e_+ o w^* - (e_- + e)x, \tag{2.3a}$$

$$\dot{y} = f_+ o^* w - (f_- + f)y, \tag{2.3b}$$

$$\dot{o} = -e_+ o w^* + e_- x + fy, \tag{2.3c}$$

$$\dot{o}^* = -f_+ o^* w + f_- y + ex \tag{2.3d}$$

for the PdPC of LuxO. Note that the form of equations (2.2a-e) implies that the reaction (2.1a) is supplemented by the irreversible reactions

$$WR_i + A_i \xrightarrow{k_i} W^* + \widehat{R}_i, \quad W^*\widehat{R}_i \xrightarrow{k_{-i}} W + R_i + A_i$$

That is, we are assuming that the autoinducer A_i can also bind to the complex WR_i, resulting in the simultaneous conversion of the receptor from a kinase to a phosphatase and LuxU to LuxU-P. For simplicity, we also take $g_i \gg k_i u_i$ and $h_i \gg k_{-i}$. (Such assumptions were also implicit in our previous work [1,5].)

The above system of equations is supplemented by the following conservation conditions:

$$W_T = w + w^* + \sum_{i=1}^{M}(v_i + v_i^*) + x + y, \tag{2.4a}$$

$$O_T = o + o^* + x + y, \tag{2.4b}$$

where W_T and O_T represent the total concentrations of proteins LuxU and LuxO, respectively.

Following the analysis of Ref. [5], we can significantly reduce the system of kinetic equations using a slow/fast analysis. First, we assume that the rates of binding and unbinding of autoinducer are sufficiently fast so that the receptors are in quasi-equilibrium:

$$r_i^{eq} = \frac{k_{-i}}{k_{-i} + k_i u_i} R_{Ti} := G_i(u_i), \quad r_i^{*eq} = R_{Ti} - r_i. \tag{2.5}$$

Since we are ignoring the feedback loop, the total concentration of receptors R_{Ti} is treated as a constant. Second, we exploit the fact that there are many more LuxU and LuxO proteins than receptors, that is, $\max\limits_{i=0,\ldots,M}\{R_{Ti}^{max}\} << W_T, O_T$, which implies $\{v_i, v_i^*\} << \{w, w^*, o, o^*\}$. Third, we assume that the irreversible reactions in equations (2.1) are fast ($f \gg f_\pm, e \gg e_\pm$), so that $\{x, y\} << \{w, w^*, o, o^*\}$. It follows that we can partition the variables according to

$$\{w, w^*, o, o^*\} \text{ slow system }, \quad \{v_i, v_i^*, x, y\} \text{ fast system.}$$

Moreover, the conservation equations (2.4) reduce to

$$W_T \approx w + w^*, \quad O_T \approx o + o^*. \tag{2.6}$$

The fast variables rapidly approach the quasi-equilibrium

$$v_i^{eq} = \frac{w}{w + K_i} r_i^{eq}, \quad v_i^{*eq} = \frac{w^*}{w^* + Qi} \widehat{r}_i^{eq}, \tag{2.7a}$$

$$x^{eq} = \frac{e_+}{e_- + e} o w^*, \quad y^{eq} = \frac{f_+}{f_- + f} o^* w, \tag{2.7b}$$

where

$$K_i = \frac{d_i + g_i}{a_i}; \quad Q_i = \frac{c_i + h_i}{b_i}. \tag{2.8}$$

The corresponding slow system then evolves according to the pair of equations (after using the conservation conditions)

$$\dot{w}^* - \dot{o}^* = \sum_{i=1}^{M} \left[\frac{g_i G_i(u_i)(W_T - w^*)}{W_T - w^* + K_i} - \frac{h_i[R_{Ti} - G_i(u_i)]w^*}{w^* + Q_i} \right], \tag{2.9a}$$

$$\dot{o}^* = ex^{eq} - fy^{eq} = \frac{e_+ e}{e_- + e}(O_T - o^*)w^* - \frac{f_+ f}{f_- + f} o^*(W_T - w^*). \tag{2.9b}$$

Finally, note that the relaxation dynamics for o^* involves products of LuxU and LuxO protein concentrations, implying that it is fast relative to w^*. We can thus set $\dot{o}^* = 0$ so that

$$\dot{w}^* = \sum_{i=1}^{M} \left[\frac{g_i G_i(u_i)(W_T - w^*)}{W_T - w^* + K_i} - \frac{h_i[R_{Ti} - G_i(u_i)]w^*}{w^* + Q_i} \right], \tag{2.10}$$

with

$$o^{*eq} = \frac{\phi O_T}{\xi(1-\phi) + \phi}, \quad \xi = \frac{f_+ f}{f_- + f} \frac{e_- + e}{e_+ e} \tag{2.11}$$

and

$$\phi = \frac{w^*}{W_T}. \tag{2.12}$$

Again we treat the slow variable ϕ as a constant during the approach to quasi-equilibrium of o^*. Note that $\xi > 0$, which guarantees that $o^{*eq} \in [0, O_T]$ with the input $\phi \in [0, 1]$. Moreover, with some algebra, one can show that o^{*eq} is a monotonically increasing function of ϕ, which makes sense, considering LuxU is a phospho-relay protein and transports the phosphate group from/to LuxO.

To simplify the following analysis, we now take $K = K_i/W_T$ and $Q = Q_i/W_T$ for all $i = 1, \ldots, M$, and non-dimensionalize time by setting $\tau = g_1 R_{T1} t/W_T$. After some algebra, one can show that [5]

$$\frac{d\phi}{d\tau} = \frac{\sum_{i=1}^{M} \Lambda_i \left[A_i(\mathbf{u})\phi^2 - B_i(\mathbf{u})\phi + C_i(\mathbf{u}) \right]}{(\phi + Q)(1 - \phi + K)}, \tag{2.13}$$

where

$$A_i(\mathbf{u}) = \frac{\beta_i \alpha_i u_i - 1}{1 + \alpha_i u_i}, \quad C_i(\mathbf{u}) = \frac{Q}{1 + \alpha_i u_i}, \tag{2.14a}$$

$$B_i(\mathbf{u}) = (1 + K)A_i(\mathbf{u}) + (1 + K/Q)C_i(\mathbf{u}), \tag{2.14b}$$

and

$$\alpha_i = \frac{k_i}{k_{-i}}, \quad \beta_i = \frac{h_i}{g_i}, \quad \Lambda_i = \frac{R_{Ti}}{R_{T1}} \frac{g_i}{g_1}. \tag{2.15}$$

Here Λ_i represents the ratio of the total concentration of pathway i receptors with the total concentration of pathway 1 receptors. Note that $\Lambda_1 \equiv 1$. Previously, we showed that Λ_i directly controls the sensitivity of signal integration [5]. We now show that when the LuxN feedback loop is included, this sensitivity is regulated by the concentration of Qrr.

2.2 sRNA and feedback kinetics

The output of the PdPC networks acts as input to the Qrr network, see Fig. 2. That is, LuxO-P binds with the qrr promoter P to activate the production of Qrr. Since we are focusing on the role of the LuxN loop, we don't distinguish between the different Qrr species, which are thus represented by the single symbol Q. As Qrr directly represses the production of the QS regulator LuxR, it follows that a higher concentration of Q indicates lower QS expression and vice versa. The basic reaction scheme is

$$P^0 \underset{k_{-p}}{\overset{k_p O^*}{\rightleftharpoons}} P^1 \xrightarrow{k_q} Q, \quad Q \xrightarrow{\gamma_q} \emptyset, \tag{2.16}$$

where LuxO-P is taken to be in quasi-equilibrium. Equation (2.16) represents the action of LuxO-P on the qss promoter P, with P^0 and P^1 denoting the inactive and active promoter states, respectively. Let $[P^0] = p^0$, $[P^1] = p^1$, $[Q] = q$ with $1 = p^0 + p^1$ (assuming a single promoter site). The corresponding kinetic equations are

$$\dot{p}^1 = k_p o^* (P_T - p^1) - k_{-p} p^1, \tag{2.17a}$$

$$\dot{q} = k_q p^1 - \gamma_q q, \tag{2.17b}$$

where k_q and γ_q are the production and degradation rates of Qrr Q. The assumption of large O_T means that (p^0, p^1) can be taken to be a fast subsystem. We thus obtain the quasi-equilibrium

$$p^{1eq} = \frac{o^{*eq}}{o^{*eq} + \eta O_T}, \quad \eta = \frac{k_{-p}}{k_p O_T}. \tag{2.18}$$

It follows that the concentration q of Qrr evolves according to

$$\frac{dq}{d\tau} = \frac{\widehat{k}_q}{1 + \eta - \eta\xi + \eta\xi/\phi} - \widehat{\gamma}_q q, \tag{2.19}$$

where we have used equation (2.11), and set

$$\widehat{k}_q = \frac{k_q W_T}{g_1 R_{T1}}, \quad \widehat{\gamma}_q = \frac{\gamma_q W_T}{g_1 R_{T1}}. \tag{2.20}$$

So far we have used a slow/fast analysis to reduce the PdPC and Qrr network kinetics to a planar dynamical system involving the pair of variables (ϕ, q), see equations (2.13) and (2.19). In the absence of feedback,

LuxU-P drives Qrr, that is, the ϕ dynamics is independent of q. Inclusion of the LuxN feedback loop means that Qrr now represses the production of the cognate receptor R_i of A_i, and we have to modify the receptor kinetic equation (2.2a), due to the fact that the total concentration of receptors is no longer constant. As we will show, this leads to the factors Λ_i in equations (2.14) picking up a dependence on q. Let X_i and M_i denote the gene and mRNA responsible for the synthesis of receptors R_i, respectively. For concreteness, we assume that the action of Qrr is to increase the degradation rate of mRNA. (The precise form of the repression does not affect the basic conclusions of the analysis.) The reaction scheme for the feedback then takes the form

$$X_i \xrightarrow{B_i} X_i + M_i, \quad M_i \xrightarrow{\gamma_{mi}(q)} \emptyset, \tag{2.21a}$$

$$M_i \xrightarrow{t_{ri}} M_i + R_{Ti}, \quad R_{Ti} \xrightarrow{\gamma_{ri}} \emptyset \tag{2.21b}$$

Here B_i and $\gamma_{mi}(q)$ are the production rate and q-dependent degradation rate of mRNA M_i, whereas t_{ri} and γ_{ri} are the production and degradation rates of R_i. Setting $[M_i] = m_i$, equation (2.2a) is replaced by the system of equations

$$\dot{r}_i = k_{-i}(R_{Ti} - r_i) - k_i r_i u_i + t_{ri} m_i - \gamma_{ri} r_i, \tag{2.22a}$$

$$\dot{m}_i = B_i - \gamma_{mi}(q) m_i, \tag{2.22b}$$

$$\dot{R}_{Ti} = t_{ri} m_i - \gamma_{ri} R_{Ti}, \tag{2.22c}$$

Again assuming that the receptor kinetics is faster than the PdPC kinetics, we can consider the quasi-equilibrium solution

$$r_i^{eq} = \frac{k_{-i} + \gamma_{ri}}{k_{-i} + \gamma_{ri} + k_i u_i} R_{Ti}^{eq}(q) \tag{2.23a}$$

where

$$R_{Ti}^{eq}(q) = \frac{t_{ri}}{\gamma_{r_i}} \frac{B_i}{\gamma_{mi}(q)} = \overline{R}_{Ti} F_i(q), \tag{2.23b}$$

and

$$\overline{R}_{Ti} = \frac{t_{ri}}{\gamma_{r_i}} \frac{B_i}{\gamma_{mi}(0)} \quad F_i(q) = \frac{\gamma_{mi}(0)}{\gamma_{mi}(q)}. \tag{2.23c}$$

Here the constant $\overline{R}_{Ti} = R_{Ti}(0)$ is the total concentration of pathway i receptors without feedback, or the maximum total concentration of pathway i receptors. Note that $0 < F_i(q) \leq 1$, and if the production of R_i is not regulated by Qrr, then $F_i(q) = 1$.

Comparison with equation (2.5) shows that the effects of feedback are two-fold: a constant shift of the effective rate constant k_{-i}, $k_{-i} \to k_{-i} + \gamma_{ri}$, and a q-dependent $R_{Ti}^{eq}(q)$. Repeating the derivation of equation (2.13) we find that

$$\frac{d\phi}{d\tau} = \frac{\sum_{i=1}^{M} \Lambda_i(q) \left[A_i(\mathbf{u})\phi^2 - B_i(\mathbf{u})\phi + C_i(\mathbf{u}) \right]}{(\phi + Q)(1 - \phi + K)}, \tag{2.24}$$

where A_i, B_i and C_i are still given by equations (2.14), $\tau = g_1\overline{R}_{T1}t/W_T$, and

$$\alpha_i = \frac{k_i}{k_{-i} + \gamma_{ri}}, \qquad \Lambda_i(q) = \frac{\overline{R}_{Ti}}{\overline{R}_{T1}}\frac{g_i}{g_1}F_i(q). \tag{2.25}$$

Note that Λ_i, the relative total concentration of pathway i receptors is now a function of q due to the LuxN feedback, whereas, Λ_i is just a constant in the absence of feedback, as shown in (2.15).

2.3 Bifurcation Analysis

In order to find the steady state values of ϕ and q as a function of the vector $\mathbf{u}$ of autoinducer concentrations, we need to solve the pair of equations

$$A(\mathbf{u}, q)\phi^2 - B(\mathbf{u}, q)\phi + C(\mathbf{u}, q) = 0 \tag{2.26a}$$

$$q = f_2(\phi) := \frac{1}{E_1 - E_2 + E_2/\phi} \tag{2.26b}$$

for $\phi \in [0, 1]$, with

$$E_1 = (1 + \eta)\widehat{\gamma}_q/\widehat{k}_q, \quad E_2 = \eta\xi\widehat{\gamma}_q/\widehat{k}_q,$$

and $A(\mathbf{u}, q) = \sum_{i=1} \Lambda_i(q)A_i(\mathbf{u})$ etc. The first equation gives

$$\phi^{eq}(\mathbf{u}, q) = \begin{cases} \dfrac{B(\mathbf{u}, q) - \sqrt{B(\mathbf{u}, q)^2 - 4A(\mathbf{u}, q)C(\mathbf{u}, q)}}{2A(\mathbf{u}, q)}, \text{ if } A(\mathbf{u}, q) \neq 0 \\ \\ \dfrac{Q}{Q + K}, \text{ if } A(\mathbf{u}, q) = 0. \end{cases} \tag{2.27}$$

Given any $\mathbf{u}$, we need to solve the following implicit equation for q^{eq},

$$H(\mathbf{u}, q) \equiv q - \frac{1}{E_1 - E_2 + E_2/\phi^{eq}(\mathbf{u}, q)} = 0. \tag{2.28}$$

It is straightforward to show that, given $\mathbf{u}$, there exists q^{eq} such that $H(\mathbf{u}, q) = 0$. First, regardless of the value of q we know that $\phi^{eq} \in [0, 1]$. Setting $q = 0$, we have

$$H(\mathbf{u}, 0) \in [-1/E_1, 0]. \tag{2.29}$$

Similarly, taking $q \to \infty$ implies $H(\mathbf{u}, q) \to \infty$, since $(E_1 - E_2 + E_2/\phi^{eq})^{-1}$ is bounded. If $H(\mathbf{u}, q) = 0$ at $q = 0$, then the proof is done. If not, we know that

$$H(\mathbf{u}, 0) < 0 < H(\mathbf{u}, \infty). \tag{2.30}$$

As $H(\mathbf{u}, q)$ is continuous in q, by the Intermediate Value Theorem, we know that there exists a $q^{eq} \in (0, \infty)$, such that $H(\mathbf{u}, q^{eq}) = 0$.

In order to determine whether or not the steady state is unique, we will carry out a bifurcation analysis. For the sake of illustration, consider

the case $M = 2$, namely, two parallel QS input pathways. (When $M > 2$, the following bifurcation analysis can be performed numerically.) Moreover, suppose that $\gamma_{mi}(q)$ is a linear function of q such that

$$\Lambda_i(q) = \frac{1}{C_i q + D_i}, \tag{2.31}$$

for constants C_i, D_i. First, we determine the ϕ-nullcline from equation (2.26a). From the definitions of A, B, C in equation (2.14), u_i is always multiplied by α_i, which indicates that we can nondimensionalize u_i by setting $\alpha_i = 1$. We also set $\beta_i = 1$ for convenience. Substituting the resulting expressions for A, B, C into the quadratic equation $A\phi^2 - B\phi + C = 0$ and reorganizing terms gives (for $M = 2$)

$$\frac{\Lambda_2(q)}{\Lambda_1(q)} = \frac{C_1 q + D_1}{C_2 q + D_2} = -\frac{1+u_2}{1+u_1}\left[\frac{h(\phi) - u_1}{h(\phi) - u_2}\right], \tag{2.32}$$

where,

$$h(\phi) = \frac{\phi^2 + (Q-1)\phi - Q}{\phi^2 - (1+K)\phi} = \frac{(\phi+Q)(\phi-1)}{\phi(\phi - 1 - K)} \geq 0. \tag{2.33}$$

For concreteness, we will study the case where only one AI pathway is controlled by qrr. Without loss of generality, we take this to be pathway $i = 2$. This means that $C_1 = 0$ and $C_2 \neq 0$. Setting $D_1 = 1$, the ϕ-nullcline is then determined by the equation

$$q = f_1(\phi) \equiv -\frac{1}{C_2}\frac{1+u_1}{1+u_2}\left[\frac{h(\phi) - u_2}{h(\phi) - u_1}\right] - \frac{D_2}{C_2}. \tag{2.34}$$

By taking the derivative of f_1, we find that

$$\frac{df_1}{d\phi} = \frac{1}{C_2}\frac{1+u_1}{1+u_2}\left[\frac{u_1 - u_2}{(h(\phi) - u_1)^2}\right]\frac{dh}{d\phi}, \tag{2.35}$$

where

$$\frac{dh}{d\phi} = -\frac{Q(\phi-1)^2 + K\phi^2 + KQ}{[\phi^2 - (1+K)\phi]^2} < 0. \tag{2.36}$$

Therefore, when $u_1 > u_2$, the function $q = f_1(\phi)$ is decreasing and when $u_1 < u_2$, the function is increasing. Let $\phi_1 = h^{-1}(u_1)$ and $\phi_2 = h^{-1}(u_2)$. It can be seen that the graph of $q = f_1(\phi)$ in the first quadrant will have the $x-$intercept $(0, \phi_2)$ and an asymptote of $\phi = \phi_1$.

Similarly, the nullcline of q is given by equation (2.26b). Calculating the derivative of the q-nullcline shows that

$$\frac{df_2}{d\phi} = \frac{E_2}{(E_1\phi - E_2\phi + E_2)^2} > 0. \tag{2.37}$$

Therefore, the graph $q = f_2(\phi)$ is a strictly increasing function. Moreover, since

$$\frac{d^2 f_2}{d\phi^2} = -\frac{2E_2(E_1 - E_2)}{(E_1\phi - E_2\phi + E_2)^3}, \tag{2.38}$$

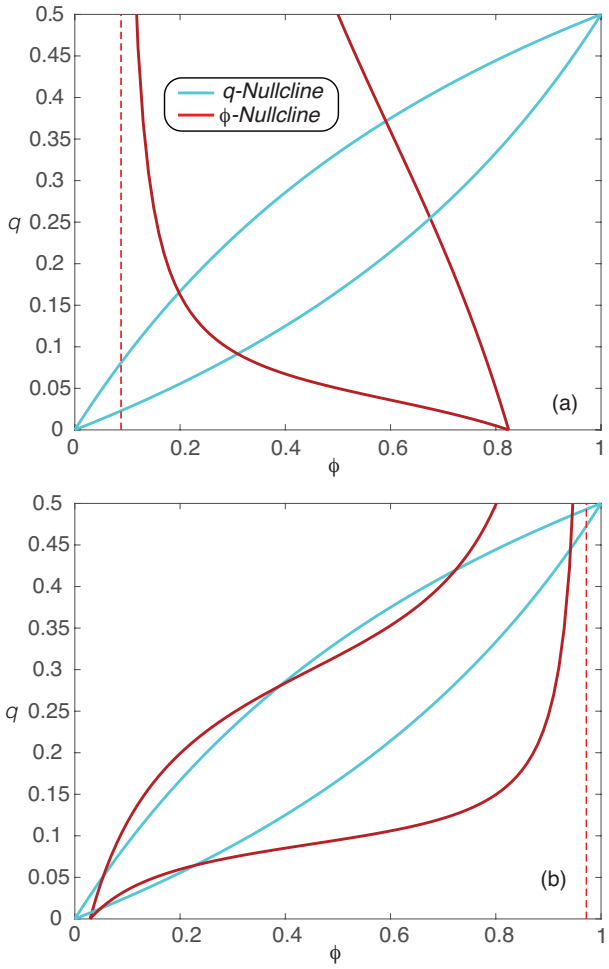


Fig. 3 Illustration of two distinct scenarios for nullcline intersections. The q-nullcline (green) is always increasing and doesn't depend on the values of u_1 and u_2. Two example q-nullclines are shown, which are obtained by setting $E_1 = 2$, $E_2 = 1$ (concave down) and $E_1 = 2, E_2 = 4$ (concave up), respectively. On the other hand, the corresponding ϕ-nullcline is decreasing when $u_1 > u_2$ (Fig. 3a) and it is increasing when $u_1 < u_2$ (Fig. 3b). For the sake of illustration, we take $K = Q = 0.1$. Also, $u_1 = 2$, $u_2 = 0.2$ in (a) and $u_1 = 0.2$, $u_2 = 5$ in (b). In both cases, we show two example ϕ-nullclines, which are obtained by setting either $D_2 = 1$, $C_2 = 2$, $C_2 = 20$ or $D_2 = 0.05$, $C_2 = 3$, $C_2 = 10$.

it follows that when $E_1 > E_2$, the graph $q = f_2(\phi)$ is concave down and when $E_1 < E_2$, the graph is concave up.

Combining our various observations, we find three distinct scenarios depending on the ranges of the AI concentrations u_1 and u_2, see Fig. 3.

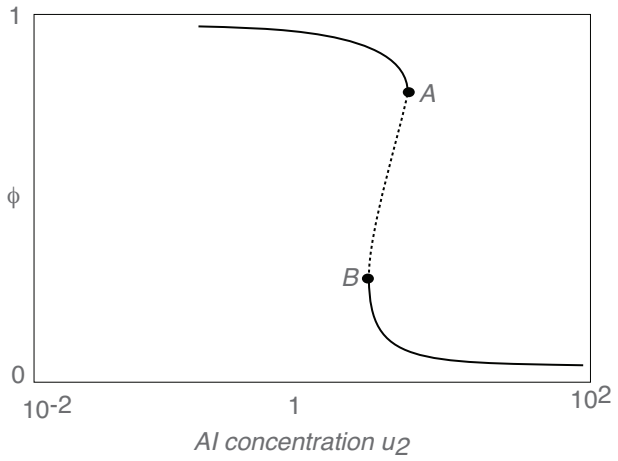


Fig. 4 Saddle-node bifurcation diagram for the system given by equations (2.24) and (2.19) with the following parameter values: $u_1 = 10^{-1}$, $C_1 = 0$, $C_2 = 3.6$, $D_2 = 0.1$, $E_1 = 2$, $E_2 = 6$, $K = Q = 0.1$, $\beta_1 = \beta_2 = 1$. At the bifurcation points B and A, we have $u_2 \approx 10^{0.63}$ and $u_2 \approx 10^{0.33}$, respectively.

Case (i): $u_1 > u_2$. $q = f_1(\phi)$ is decreasing and $q = f_2(\phi)$ is increasing, which implies that the two functions can intersect no more than once. With existence established at the beginning of section 2.3, we know that there exists a unique equilibrium. Moreover, with some algebra, one can show the equilibrium is globally stable.

Case (ii): $u_1 = u_2$. When both autoinducers have the same concentration, $u_1 = u_2$, we have

$$f_1(\phi) = -\frac{1}{C_2} - \frac{D_2}{C_2}. \tag{2.39}$$

Therefore, $q = f_1(\phi)$ is a constant function, which guarantees the uniqueness of the intersection/equilibrium. Again it can be established that the equilibrium is globally stable.

Case (iii): $u_1 < u_2$. This is the case where uniqueness is not guaranteed, because both functions f_1 and f_2 are increasing. Indeed, when $u_1 < u_2$, multiple equilibria exist, which is illustrated in Fig. 4.

In the following, we will restrict our analysis to the parameter regions with a unique equilibrium. In appendix A, we show that a sufficient condition for this to hold is

$$\frac{1+K}{1+K+Q} < \phi < 1. \tag{2.40}$$

In the remainder of the paper, we take $K = 1$ and $Q = 10$, and restrict u_1 and u_2 so that the ϕ response satisfies (2.40) so that there exists a globally stable equilibrium.

2.4 LuxN feedback as a Weight Control Mechanism

In our previous work [5] we showed how an asymmetry in the total concentration of receptors of the different AIs, $R_{T_1} \neq R_{T_2}$, leads to a corresponding asymmetry in signal integration. In other words, the system is more sensitive to the presence of one AI over another. In our LuxN feedback model, the

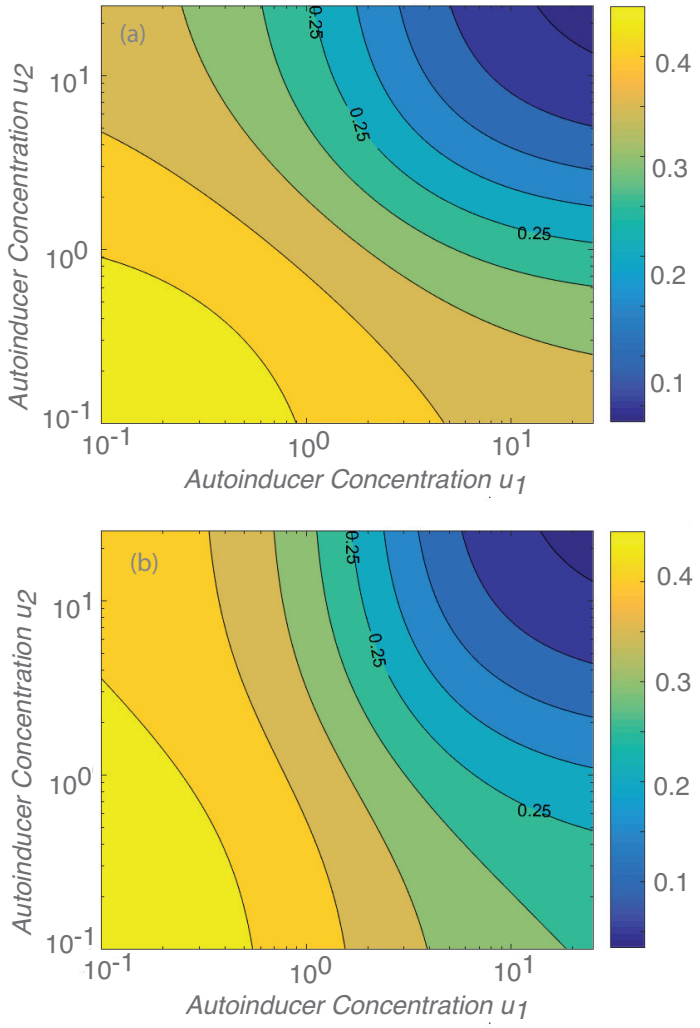


Fig. 5 Contour plots of qrr response q with (a) no LuxN feedback loop, (b) a LuxN-feedback loop in pathway $i = 2$. The non-dimensionalized parameters used in this plot are: $\alpha_1 = \alpha_2 = 1$, $\beta_1 = \beta_2 = 1$, $K = 1$, $Q = 10$, $E_1 = 2$, $E_2 = 6$, and $C_1 = 0$, $D_2 = 1$. (a) $C_2 = 0$; (b) $C_2 = 3.6$.

total receptor concentrations are determined dynamically, which provides a possible mechanism for changing the direction of the biased response based on the QS state q.

Suppose that in the absence of feedback ($q = 0$), $\overline{R}_{T_1} = \overline{R}_{T_2}$, which can be implemented by setting $D_1 = D_2 = 1$. Having $\overline{R}_{T_1} = \overline{R}_{T_2}$ means the

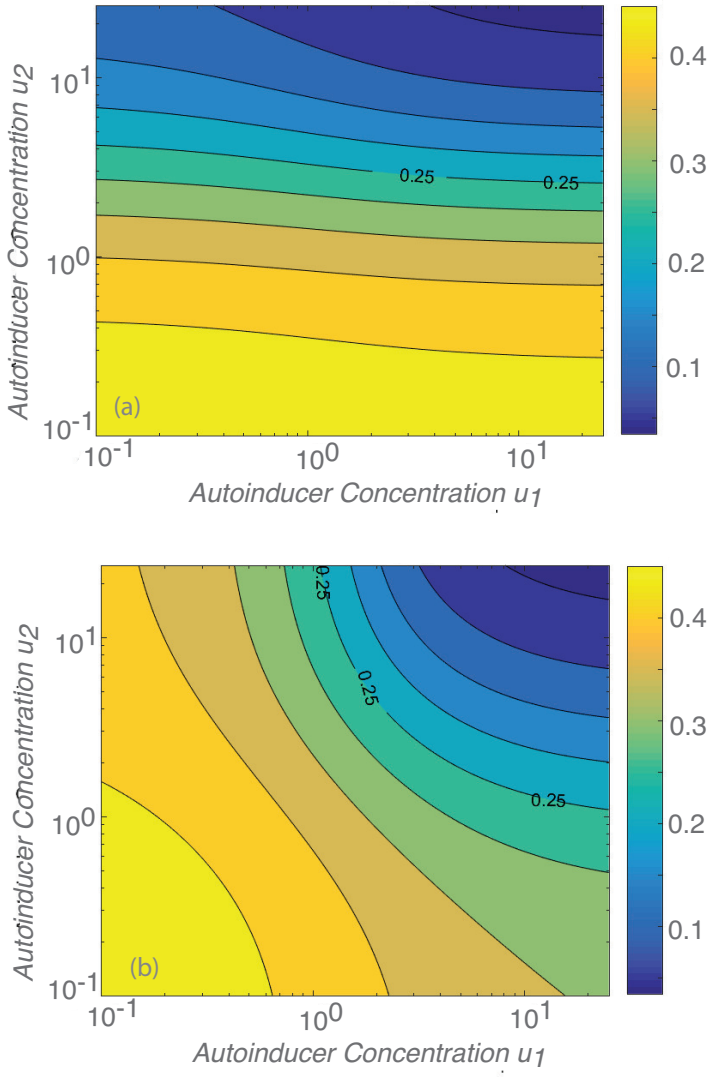


Fig. 6 Same as Fig. 5 except that $D_2 = 0.1$. (a) In the absence of feedback the system is more sensitive to u_2 and the contour lines are almost horizontal. (b) LuxN feedback counteracts the asymmetry in response, particularly at high levels of q^{eq}.

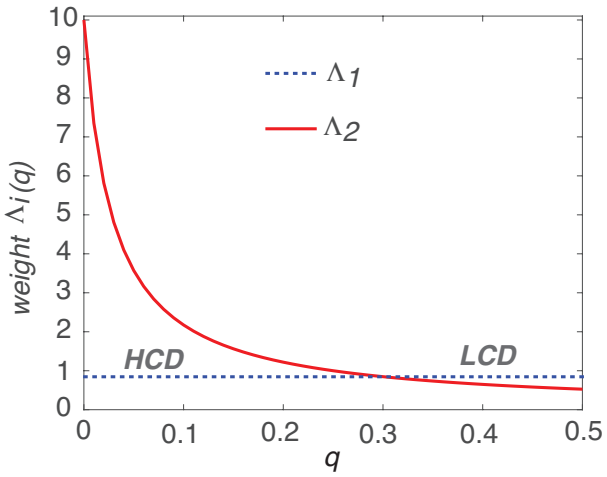


Fig. 7 LuxN feedback allows bacteria to actively control the weight of each pathway. Suppose that QS turns on when $q < q_\theta$, with $q_\theta = 0.25$. Let $C_1 = 0, D_1 = 1$ and $C_2 = 3.6, D_2 = 0.1$, so that LuxN feedback only acts on pathway 2 receptors. It follows that the total concentration of pathway 1 receptors is independent of q, while q actively controls the total receptor concentration of pathway 2. We pick values of C_i and D_i so that the following holds. At low cell density (LCD), for which $q > q_\theta$, we have $\Lambda_2(q) < \Lambda_1(q)$ and the system is biased towards pathway 1. On the other hand, at high cell density (HCD), when $q < q_\theta$, we have $\Lambda_2 > \Lambda_1$ and the system is biased towards pathway 2.

sensitivity with respect to A_1 and A_2 are the same without feedback. Figure 5 illustrates how LuxN feedback breaks the symmetry of the *qrr* response. In the absence of feedback, Figure 5(a), the *qrr* response is symmetric with respect to the two AI signals. On the other hand, in the presence of feedback, Figure 5(b), *qrr* actively represses the production of pathway 2 receptors, leading to a weaker discrimination of A_2. This is reflected by the observation that the contour lines are more vertical.

In Figure 5, the maximum concentration of pathway 1 and pathway 2 receptors are the same, and LuxN feedback only acts on the latter. It follows from equations $(2.23b - 2.23c)$ that $R^{eq}_{T1}(q) = \overline{R}_{T1}(0) = \overline{R}_{T2}(0) > R^{eq}_{T2}(q)$. Therefore the concentration of pathway 1 receptors will always be greater than the concentration of pathway 2 receptors , which leads to a fixed bias towards pathway 1 for all values of q. If we now break the assumption of $\overline{R}_{T_1} = \overline{R}_{T_2}$, it is also possible for feedback to actively change the direction of the bias. That is, suppose $\overline{R}_{T1}(0) < \overline{R}_{T2}(0)$, which can be imposed by setting $D_2 < 1$. The LuxN feedback is still taken to act on pathway 2 receptors alone. Hence, pathway 2 starts with more receptors when $q = 0$. However, as q increases, the concentration of pathway 2 receptors eventually drops below the concentration of pathway 1 receptors, where the latter is constant with respect to q. The above scenario is illustrated in Fig. 6. In the absence of feedback, the response contours are insensitive to the

concentration of A_1, whereas sensitivity to A_1 is recovered when feedback to pathway 2 is included; this effect is stronger for larger q values.

From a mathematical modeling perspective, we can understand the effects of LuxN feedback in terms of its active control on the relative total receptor concentration of pathway i, $\Lambda_i(q)$, or what we call the 'weight function', see equation (2.31). The latter indicates that C_2 measures the strength of the negative feedback, whereas $D_2 \propto \overline{R}_{T_1}/\overline{R}_{T_2}$ represents the ratio between the maximum total receptor concentration of pathway 1 with the maximum receptor concentration of pathway 2. As we discussed previously, when there is no feedback for any pathway, $C_i = 0$ for $i = 1, 2$, and $\Lambda_i(q)$ is a constant function with respect to q. Therefore, each pathway has a fixed weight for any value of q, or at both low and high cell densities. On the other hand, if pathway 2 is controlled by LuxN feedback, then the pathway 2 weight depends on q. Therefore, plotting the both $\Lambda_1(q)$ and $\Lambda_2(q)$ gives us a direction indicator of at different value of q, which pathway is weighted more. This is illustrated through an example in Fig. 7, which indicates that LuxN feedback directly controls the weight of pathway 2, so that the relative weights of the two pathways can change based on the value of q. Note that we can think of q value, the qrr concentration, as a indicator QS-measure population level. That is, high q value corresponds to a low cell density (LCD) at the population level and low q value corresponds to a high cell density (HCD).

3 Population Model with LuxN Loop

We now consider a population model with N identical cells, where every cell detects M different autoinducers and all cells are coupled by the extracellular environment via free diffusion of the autoinducer molecules. In order to extend the analytical results of section 2, we take $M = 2$. (The generalization to cases $M > 2$ would need to be performed numerically.) Let i, $i = 1, 2$, be the index of the AI type and μ, $\mu = 1, \ldots, N$, be the index of the cell number. In order to keep the number of equations under control, we introduce the vectors

$$\mathbf{X}_i = (v_i, v_i^*, w, w^*)^\top, \ \mathbf{Y} = (o, o^*, x, y)^\top,$$
$$\mathbf{Z}_i = (r_i, R_{Ti}, m_i, q, p^0, p^1)^\top,$$

and we rewrite the single-cell model in a more compact form

$$\dot{\mathbf{X}}_i = \mathcal{X}_i(\mathbf{X}_i, \mathbf{Y}, r_i, R_{Ti}) \tag{3.1a}$$
$$\dot{\mathbf{Y}} = \mathcal{Y}(\mathbf{Y}, w, w^*) \tag{3.1b}$$
$$\dot{\mathbf{Z}}_i = \mathcal{Z}_i(\mathbf{Z}_i, o^*). \tag{3.1c}$$

Here equation (3.1a) corresponds to the system (2.2b-e), equation (3.1b) corresponds to the system (2.3a-d), and equation (3.1c) corresponds to the systems (2.17a-b) and (2.22a-c). The population-level version of the above

equations can now be written down by adding the label μ to all of the dynamical variables and using the fact that all cells are taken to be identical:

$$\dot{\mathbf{X}}_{i\mu} = \mathcal{X}_i(\mathbf{X}_{i\mu}, \mathbf{Y}_\mu, r_{i\mu}, R_{Ti\mu}) \tag{3.2a}$$
$$\dot{\mathbf{Y}}_\mu = \mathcal{Y}(\mathbf{Y}_\mu, w_\mu, w_\mu^*) \tag{3.2b}$$
$$\dot{\mathbf{Z}}_{i\mu} = \mathcal{Z}_i(\mathbf{Z}_{i\mu}, o_\mu^*). \tag{3.2c}$$

These are supplemented by equations describing the diffusive exchange of AI with the extracellular environment:

$$\dot{U}_i = \rho\kappa_i(u_{av}^i - U_i) - \gamma_i U_i, \tag{3.3a}$$
$$\dot{u}_{i\mu} = \Gamma_i + k_{-i}(R_{Ti\mu} - r_{i\mu}) - k_i r_{i\mu} u_{i\mu} - \kappa_i(u_{i\mu} - U_i), \tag{3.3b}$$

where U_i is the concentration of A_i in the extracellular environment, and

$$u_{av}^i = \frac{1}{N}\sum_{\mu=1}^{N} u_{i\mu}. \tag{3.4}$$

In contrast to the single-cell model, the intracellular AI concentrations are dynamical variables, with κ_i the rate of diffusive exchange of A_i between the interior of a cell and the extracellular domain, Γ_i the internal production rate of A_i, and γ_i the degradation rate of extracellular A_i. Finally, $\rho = Nv_{cyt}/V_{ext}$ represents the cell density in terms of the ratio of total cytosolic volume v_{cyt} and the extracellular volume V_{ext}, with N the total number of cells [1,5]. In this model, the cell density is the external input to the population rather than the AI concentrations of the single-cell model.

We now want to show that the solution of each cell j in the population model globally converges to a synchronized state. First, we observe that equations (3.3a,b) drive equations (3.2). Therefore we can decouple $(U_i, u_{i\mu})$ from $(\mathbf{X}_{i\mu}, \mathbf{Y}_\mu, \mathbf{Z}_{i\mu})$. Hence, we can perform the same fast-slow analysis in section 2 on sub-system $(\mathbf{X}_{i\mu}, \mathbf{Y}_\mu, \mathbf{Z}_{i\mu})$, leading to the reduced system of equations (2.24) and (2.19) for each pair (ϕ_μ, q_μ). Therefore, we have the reduced population system $(U_i, u_{i\mu}, \phi_\mu, q_\mu)$ with $U_i, u_{i\mu}$ evolving according to the equations

$$\frac{dU_i}{d\tau} = \rho\kappa_i(u_{av}^i - U_i) - \gamma_i U_i, \tag{3.5a}$$
$$\frac{du_{i\mu}}{d\tau} = \Gamma_i - \kappa_i(u_{i\mu} - U_i), \tag{3.5b}$$

$$\frac{d\phi_\mu}{d\tau} = \frac{\sum_{i=1}^{M} \Lambda_i(q_\mu)\left[A_i(\mathbf{u}_\mu)\phi_\mu^2 - B_i(\mathbf{u}_\mu)\phi_\mu + C_i(\mathbf{u}_\mu)\right]}{(\phi_\mu + Q)(1 - \phi_\mu + K)}, \tag{3.5c}$$

$$\frac{dq_\mu}{d\tau} = \frac{\widehat{k}_q}{1 + \eta - \eta\xi + \eta\xi/\phi_\mu} - \widehat{\gamma}_q q_\mu, \tag{3.5d}$$

Note that we have rescaled κ_i,γ_i and Γ_i in order to use the dimensionless time variable τ.

Following our previous work [1,5], we can use the partial contraction theorem of Ref. [24] to investigate the global convergence properties of the reduced population model. The basic idea is to consider the reduced non-autonomous *virtual* single-cell system (u_i, ϕ_i, q_i),

$$\frac{du_i}{d\tau} = \Gamma_i - \kappa_i(u_i - U_i(\tau)), \tag{3.6a}$$

$$\frac{d\phi}{d\tau} = \frac{\sum_{i=1}^{M} \Lambda_i(q)\left[A_i(\mathbf{u})\phi^2 - B_i(\mathbf{u})\phi + C_i(\mathbf{u})\right]}{(\phi+Q)(1-\phi+K)}, \tag{3.6b}$$

$$\frac{dq}{d\tau} = \frac{\widehat{k}_q}{1+\eta-\eta\xi+\eta\xi/\phi} - \widehat{\gamma}_q q, \tag{3.6c}$$

where $U_i(\tau)$ is treated as an arbitrary external input. After some algebra, we find that the Jacobian matrix J of the resulting system has the following form:

$$J = \begin{bmatrix} -\kappa_i & \mathbf{0} \\ J_{12} & J_{22} \end{bmatrix}, \tag{3.7}$$

where J_{22} represents the Jacobian of the $\phi - q$ subsystem. Since $-\kappa_i < 0$, to show all eigenvalues of J have negative real part, we just need to show that all eigenvalues of J_{22} have negative real part. Since $M = 2$, we can apply the analysis of section 2.3. The latter showed that the $\phi - q$ subsystem has a unique globally stable equilibrium, which implies that all eigenvalues of its Jacobian J_{22} have negative real part. Finally, since (3.6a) is linear in $U_i(\tau)$, the full system (3.6) is contracting, which means that any two trajectories, starting from different initial conditions, converge exponentially to each other. We then note that setting $\Theta_i = \Theta_{i\mu}$ in the virtual system recovers the dynamics of the μth cell, where

$$\Theta_i = (u_i, \phi, q), \quad \Theta_{i\mu} = (u_{i\mu}, \phi_\mu, q_\mu).$$

Hence, $\Theta_{i\mu}$ for $\mu = 1, \ldots, N$ are particular solutions of the virtual system so that if the virtual system is contracting in Θ_i, then all of the solutions $\Theta_{i\mu}$, $\mu = 1, \ldots, N$ converge exponentially toward each other. It follows that in the asymptotic limit $t \to \infty$, we effectively have a single cell diffusively coupled to the extracellular medium, that is $\Theta_{i\mu}(t) \to \Theta_i(t)$.

In conclusion, ignoring transients, the population model reduces to an effective single-cell model given by equations (3.6) and (3.5a) with $u^i_{\rm av} = u_i$. These equations have the unique stable fixed point

$$u_i^{eq} = \frac{\Gamma_i}{\gamma_i}\rho + \frac{\Gamma_i}{\kappa_i} := \psi_i(\rho). \tag{3.8}$$

Finally q^{eq} is determined from equation (2.28) on setting $\mathbf{u} = \mathbf{u}^{eq}$,

$$H(\mathbf{u}^{eq}, q^{eq}) = 0. \tag{3.9}$$

We will use the bifurcation analysis of section 2.3, where we restricted the parameter region so that condition (2.40) is satisfied. It then follows that there exists a unique stable equilibrium (ϕ^{eq}, q^{eq}). In the following, we will consider how the feedback affects the QR system's response to multiple environmental inputs.

4 One-Population Model with Mass Transfer: Switch Between QS and DS

In our previous work [5], we demonstrated that QS can be used both as a population sensing mechanism and as a diffusion sensing mechanism. We recap the basic idea here. Although there have been major advances in identifying the cellular mechanisms underlying QS in various bacterial species, there is still some controversy concerning the functional significance of QS [12,23,30,21]. The classical picture is that QS allows bacteria to sense and respond appropriately to different levels of bacterial population density. The leading alternative alternative hypothesis is diffusion sensing (DS), which posits that variation in the concentration of extracellular signaling molecules is mainly determined by physical mass transfer effects such as diffusion or advection, rather than bacterial density, see Fig. 8. One argument for DS is that in natural environmental settings, bacterial growth tends to occur at much lower densities than under laboratory conditions, so that the primary information encoded by variation in signal concentration is variation in the mass transfer properties of the local environment [23].

Irrespective of whether the QS or DS viewpoint is more appropriate, it is clear that the occurrence of two environmental factors, namely, cell density and mass transfer, means that determining one of these quantities by sensing an autoinducer concentration can be confounded by the presence of the other. For example, high-density, high mass transfer environments may be indistinguishable from low-density, low mass transfer environments. In certain cases this may not be a problem, particularly if the QS system up-regulates the gene expression of secretory molecules that exert direct control over the environment [12]. That is, only high extracellular signal concentrations will lead to high concentrations of costly secreted enzymes, and this will occur under the favorable combination of low mass transfer rates and high population densities. In other words, the QS system simply needs to detect the regime of high density/low mass transfer.

In the following analysis, we extend the one-population model with mass transfer rate ω from Ref. [5] to include a *qrr*-LuxN feedback loop, and show that the latter allows the bacteria to switch between QS and DS. In order to include mass transfer, we simply replace equation (3.3a) by the following:

$$\dot{U}_i = \rho\kappa_i(u^i_{av} - U_i) - (\gamma_i + \omega)U_i. \tag{4.1}$$

Since the only difference compared with the original one-population system is replacing parameter γ_i with $\gamma_i+\omega$, we can perform a similar proof to show

that the cells of the population model with mass-transfer are synchronized, with a unique stable equilibrium, q^{eq} satisfying

$$H(\mathbf{u}^{eq}, q^{eq}) = 0, \tag{4.2}$$

where,

$$u_i^{eq} = \frac{\Gamma_i}{\gamma_i + \omega}\rho + \frac{\Gamma_i}{\kappa_i}. \tag{4.3}$$

As discussed in previous work [2,5], one way for bacteria to detect mass transfer effects in the extracellular environment, is to employ a combination of a durable signal (an AI with slow synthesis and decay) and a fragile signal (an AI with fast synthesis and decay). Fluctuations due to mass transfer won't significantly influence the presence of the fragile signal, but will affect the durable signal. In other words, the fragile signal only responds to population density, whereas the durable signal responds to both population density and mass transfer. Integration of the two signals thus allows the bacteria to recognize the mass transfer effect, which is an example of DS. In the following we will combine the idea of DS with the weight control mechanism to show that LuxN feedback allows bacteria to turn OFF or ON

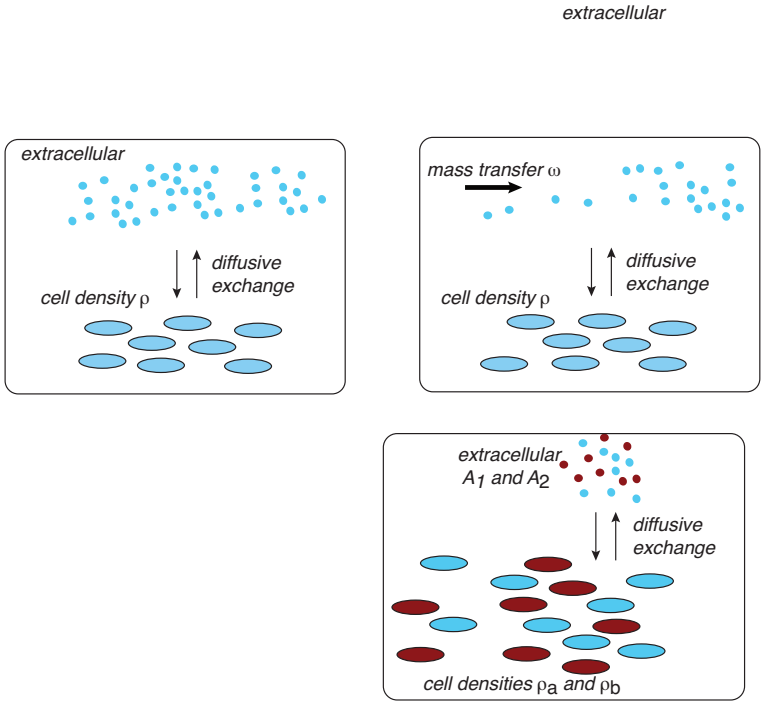


Fig. 8 Schematic diagram showing a population of bacteria producing and exchanging signaling molecules A_1 and A_2 with the extracellular environment in the presence of mass transfer effects. The level of LuxR and qrr will depend on cell density ρ and the rate of mass transfer ω.

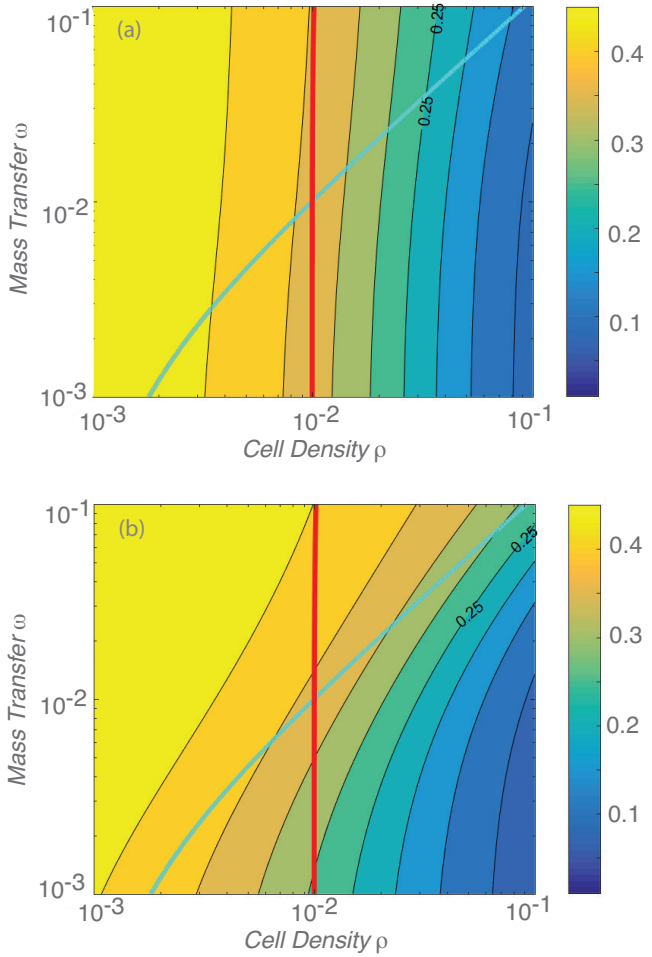


Fig. 9 One-population model with mass transfer and LuxN feedback in pathway 2. Comparison of a fixed weight scheme (no feedback) vs an adaptive weight scheme (with feedback). The thick blue line (durable signal) and red line (fragile signal) represent the curves $u_1^{eq} = \theta$ and $u_2^{eq} = \theta$, respectively, for some threshold θ, see equation (4.3). The contour plots describe how qrr responds to both population density (QS) and mass transfer (DS). (a) The fixed weight scheme is achieved by having different relative concentrations of receptors, $\overline{R}_{T2} = 10\overline{R}_{T1}$. This favors the fragile signal resulting in QS. (b) The adaptive weight scheme also includes the LuxN feedback loop to actively control the weight of different pathways during signal integration. This changes the sensitivity of the system as a function of q. The nondimensionalized parameters are same as Fig. 5, except $\gamma_1 = 0.001$, $\gamma_2 = 1$, $\Gamma_1 = 0.5$, $\Gamma_2 = 500$.

its DS function based on the state of QS. We will assume that autoinducer

$A1$ is the durable signal and $A2$ is the fragile signal. That is, we consider $A2$ as the QS detector and $A1$ as the DS detector.

In Fig. 9, we show the q-response to cell density and mass transfer in a one population model for which the total amount of receptors satisfies $\overline{R}_{T2} = 10\overline{R}_{T1}$. In the absence of feedback, the signal sensitivity shifts from autoinducer $A1$ (blue) to autoinducer $A2$ (red), as indicated by the vertical contours. The system thus implements QS. On the other hand, when feedback is included, the response depends on the level of the qrr concentration q. When q is large (LCD), the production of receptors in pathway 2 is repressed, which leads to the bias towards the durable signal A_1 and DS. As q decreases (HCD), the sensitivity switches back to the fragile signal A_2 and QS, where we can observe the continuous shift of the contour lines from diagonal to vertical. Such adaptive behavior could benefit a bacterial population. It helps the bacteria to have a higher recognition of both social and physical environments. At low cell densities, mass transfer will dominate the extracellular concentration suggesting that bacteria should increase their sensitivity to fluctuations in the extracellular environment and avoid wasting energy to produce and secrete AI and other molecules. This is much less of an issue at high cell densities.

5 Two-Population Model: Recognition of Bacteria Specificity

In this section, we extend our previous work on a two-population model [5] by including the qrr-LuxN feedback loop, and show how bacteria can employ the weight control scheme to recognize different bacteria species. It follows that all intracellular variables have an additional index for the population label, which we will take to be a or b. For concreteness, we will assume that population a synthesizes A_1 and population b synthesizes A_2, but both cell types detect A_1 and A_2, see Fig. 10. Equation (3.3a) becomes

$$\dot{U}_i = \kappa_i(\rho^a u_{av}^{ai} + \rho^b u_{av}^{bi} - \rho U_i) - \gamma_i U_i, \tag{5.1}$$

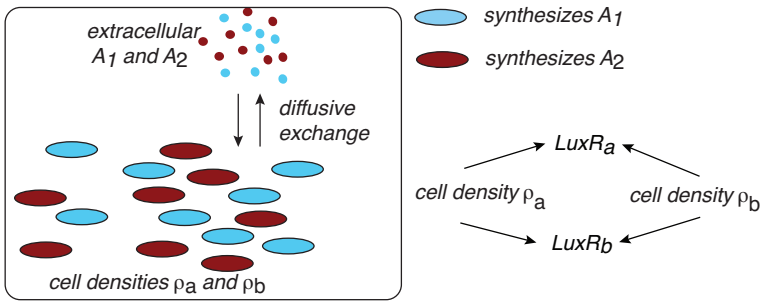


Fig. 10 Two-population model with cell densities ρ_a, ρ_b, producing and sensing two types of autoinducer A_1 and A_2, which are exchanged with the extracellular environment. Shown is the limiting case where population a produces A_1 and population b produces A_2. However, all cells detect both A_1 and A_2.

for $i = 1, \ldots, M$, with

$$u_{av}^{li} = \frac{1}{N_l} \sum_{j=1}^{N_\mu} u_{ij}^{l}, \quad l = a, b, \tag{5.2}$$

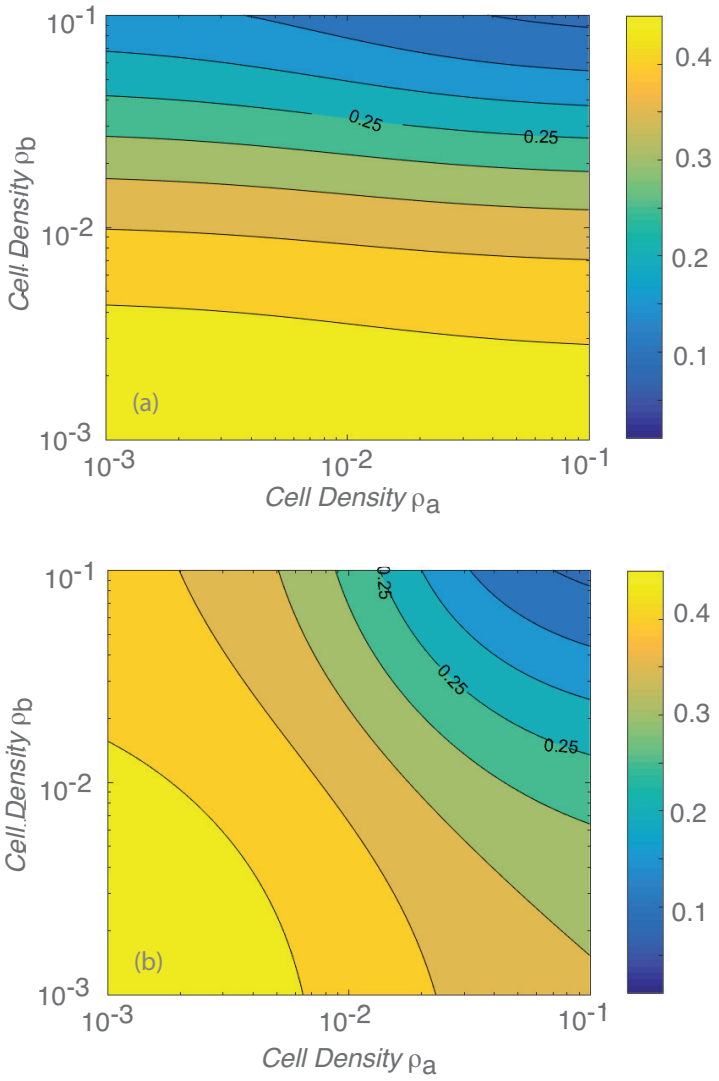


Fig. 11 Two-population model with cell densities ρ_a and ρ_b, respectively, and LuxN feedback in pathway 2. Population a produces A_1 and population b produces A_2 while both types of cells detect both A_1 and A_2, see Fig. 10. Contour plots indicate the q-response of population a. (a) Fixed weight scheme (no feedback) in which both populations are biased to detecting population a. (b) Adaptive weight scheme (feedback in pathway 2). The nondimensionalized parameters are the same as Fig. 5, except that $\Gamma_1^a = 1$, $\Gamma_2^a = 0$, $\Gamma_1^b = 0$, $\Gamma_2^b = 1$, $\gamma_1 = \gamma_2 = 0.011$.

where ρ^a, ρ^b are the two cell densities with $\rho^l = N_l v_{cyt}/V_{ext}$, $l = a, b$. It is straightforward to show that the two-population model with feedback has the appropriate contraction properties so that the system converges to a two-cell model given by two copies of equations (3.2), labeled by $\mu = a, b$, respectively, and

$$\dot{U}_i = \kappa_i(\rho^a u_i^a + \rho^b u_i^b - (\rho^a + \rho^b)U_i) - \gamma_i U_i, \tag{5.3}$$

for $i = 1, \ldots, M$. The equilibrium AI concentrations are given by

$$u_i^{l,eq} = \frac{\rho^a \Gamma_i^a + \rho^b \Gamma_i^b}{\gamma_i} + \frac{\Gamma_i^l}{\kappa_i}. \tag{5.4}$$

In Fig. 11 we plot the q-response of population a without and with feedback in pathway 2. We assume that both populations are biased towards detecting A_2 in the absence of feedback, so that the contour lines are approximately horizontal, indicating lack of sensitivity to the density ρ_a. On the other hand, in the presence of feedback, the cells tend to be sensitive to population a for large q but sensitive to both population densities for small q. Such a switch in sensitivity can be observed by the contour line slope getting flatter as the degree of QS increases. Given that different autoinducers carry species specific information, this mechanism allows QS to focus on different species at different stages of population growth, which is useful for intraspecies and interspecies bacterial communication.

6 Discussion

In this paper, we have shown how a LuxN feedback loop allows bacteria to actively switch sensitivity towards different types of autoinducers by changing the relative weight of each pathway. Such a weight control mechanism could allow the bacteria to adapt their sensitivity to different level of cell density, which has also been observed experimentally [27]. Moreover, we proposed two extensions of the population model that explore the potential functionality of the weight control mechanism. In particular, we showed how such a mechanism permits bacteria to adapt their sensitivity to additional social and physical environmental cues, thus providing a possible explanation of the role of the 'many-to-one' circuit in *V. harveyi*. We also discovered an additional consequence of adding a LuxN feedback loop, namely, that the QS response is bistable in certain parameter regimes. In future work we hope to explore this source of bistability in more detail. In particular, we want to test whether or not the bistable parameter region can be verified by multi-pathway QS bacteria such as *V. harveyi* and *V. cholera*, and its possible role in bet hedging in the presence of noise. (Biological bet hedging refers to the presence of bimodality at the population level, in which one subpopulation is less fit under typical conditions but exhibits increased fitness under stressful conditions [25].) One limitation of our current model is that it does not incorporate possible spatial effects in

QS. In particular, extracellular diffusion is assumed to be sufficiently fast so that the extracellular autoinducer concentration is uniform across all cells. In order to take into account spatial fluctuations and heterogeneities, it will be necessary to explicitly model extracellular diffusion and how it couples to cellular compartments via appropriately chosen boundary conditions.

Acknowledgements

PCB was supported by the National Science Foundation (DMS-1613048). GF was supported by the National Science Foundation (DMS-RTG 1148230).

Appendix A

In this appendix, we show that a sufficient condition for the equilibrium of the single-cell model to be unique is given by equation (2.40). We already showed the uniqueness for the cases of $u_1 > u_2$ and $u_1 = u_2$, in section 2.3. Next, we will work on the case of $u_1 < u_2$. Since the equilibrium satisfies $f_1(\phi) = f_2(\phi)$, it follows after some algebra that

$$\begin{aligned}\frac{u_2 - h(\phi)}{u_2 + 1} &= \left[\frac{\phi C_2 E_q}{(1+\eta-\eta\xi)\phi + \eta\xi} + D_2\right]\frac{h(\phi) - u_1}{1+u_1} \\ &\equiv f_3(\phi). \end{aligned} \tag{A.1}$$

Note that

$$\frac{\phi C_2 E_q}{(1+\eta-\eta\xi)\phi + \eta\xi} + D_2 = \frac{\phi C_2 E_q}{(1+\eta)\phi + \eta\xi(1-\phi)} + D_2 > 0. \tag{A.2}$$

Here, because the two sides of $(A.1)$ have to be the same sign, we have the following cases,

$$u_1 < h(\phi) < u_2, \quad u_1 = h(\phi) = u_2 \quad \text{or} \quad u_1 > h(\phi) > u_2. \tag{A.3}$$

Since we are studying the case $u_1 < u_2$, it follows that $u_1 < h(\phi) < u_2$, which implies $f_3(\phi) > 0$.
By some algebra on equation $(A.1)$, we get

$$u_2 = f_4(\phi) \equiv \frac{h(\phi) + f_3(\phi)}{1 - f_3(\phi)}. \tag{A.4}$$

Recall from equation (2.33) that $h(\phi) \geq 0$. Since the AI concentration $u_2 \geq 0$, we have $1 - f_3(\phi) > 0$. Uniqueness is guaranteed by the monotonicity of the function $f_4(\phi)$. By taking the derivative with respect to ϕ of $u_2 = f_4(\phi)$, we find

$$f_4' = \frac{df_4}{d\phi} = \frac{h'(1-f_3) + f_3'(1+h)}{(1-f_3)^2}, \tag{A.5}$$

where,

$$h' = \frac{dh}{d\phi} = -\frac{Q(\phi-1)^2 + K\phi^2 + KQ}{[\phi^2 - (1+K)\phi]^2} < 0, \tag{A.6a}$$

$$f_3' = \frac{df_3}{d\phi} = \frac{C_2 E_q \eta\xi}{[(1+\eta-\eta\xi)\phi + \eta\xi]^2}\frac{h(\phi)-u_1}{1+u_1} + \left(\frac{\phi C_2 E_q}{(1+\eta-\eta\xi)\phi+\eta\xi} + D_2\right)\frac{h'(\phi)}{1+u_1}. \tag{A.6b}$$

Since $0 < f_3 < 1$ and $1 + h > 0$, one sufficient condition for $f_4' < 0$ to be true is having $f_3' < 0$. Also,

$$\begin{aligned} f_3' &< \frac{C_2 E_q \eta\xi}{[(1+\eta-\eta\xi)\phi+\eta\xi]^2}\frac{h(\phi)}{1+u_1} + \frac{\phi C_2 E_q}{(1+\eta-\eta\xi)\phi+\eta\xi}\frac{h'(\phi)}{1+u_1}, \\ &= \frac{C_2 E_q (1+\eta)\phi^2 h'(\phi)}{[(1+\eta-\eta\xi)\phi+\eta\xi]^2(1+u_1)} + \frac{C_2 E_q \eta\xi(h(\phi) - h'(\phi)\phi^2 + \phi h'(\phi))}{[(1+\eta-\eta\xi)\phi+\eta\xi]^2(1+u_1)}, \\ &< \frac{C_2 E_q \eta\xi}{[(1+\eta-\eta\xi)\phi+\eta\xi]^2(1+u_1)}[h(\phi) - h'(\phi)\phi^2 + \phi h'(\phi)]. \end{aligned} \tag{A.7}$$

Since $0 \le \phi \le 1$, we require $h(\phi) - h'(\phi)\phi^2 + \phi h'(\phi) < 0$. By direct substitution, we have

$$h(\phi) - h'(\phi)\phi^2 + \phi h'(\phi) = \frac{(\phi-1)[(1+Q+K)\phi - (1+K)]}{(\phi - 1 - K)^2}. \tag{A.8}$$

Therefore, equation (2.40) is a sufficient condition for the response to be unique.

References

1. Bressloff PC (2016) Ultrasensitivity and noise amplification in a model of V. harveyi quorum sensing. Phys. Rev. E 93: 062418.
2. Cornforth DM, Popat R, McNally L, Gurney J, Scott-Phillips DM, Ivens A, Diggle SP, Brown SP (2014) Combinatorial quorum sensing allows bacteria to resolve their social and physical environment. Proc. Natl. Acad. Sci. USA 111:4280-4284.
3. Davies DG, Parsek MR, Pearson JP, Iglewski BH, Costerton JW, Greenberg EP (1998) The involvement of cell-to-cell signals in the development of bacterial biofilm. Science 280:295-298).
4. Dunlap PV (1999) Quorum regulation of luminescence in Vibrio fischeri. J. Mol. Microbiol. Biotechnol. 1:5-12.
5. Fan G, Bressloff PC (2017) Population Model of quorum sensing with multiple parallel pathways. Bull. Math. Biol. 79:2599-2626.
6. Fuqua C, Winans SC, Greenberg EP (1996) Census and consensus in bacterial ecosystems: the LuxR-LuxI family of quorum-sensing transcriptional regulators. Annu. Rev. Microbiol. 50:727-751.

7. Ge H, Qian M (2008) Sensitivity amplification in the phosphorylation-dephosphorylation cycle: nonequilibrium steady states, chemical master equation and temporal cooperativity. J. Chem. Phys. 129:015104.
8. Goldbeter A, Koshland DE (1981) An amplified sensitivity arising from covalent modification in biological systems. Proc. Natl. Acad. Sci. USA 78:684-6844.
9. Golub GH, Loan, CF (1996) Matrix Computations, Baltimore: Johns Hopkins University Press.
10. Goryachev AB (2009) Design principles of the bacterial quorum sensing gene networks. WIRE Syst. Biol. Med. 1:45-60.
11. Haseltine EL, Arnold FH (2008) Implications of rewiring bacterial quorum sensing. Appli. Env. Microbiolo. 74(2): 437-445.
12. Hense BA, Kuttler C, Muller J, Rothballer M, Hartmann A, Kreft JU (2007) Does efficiency sensing unify diffusion and quorum sensing? Nat. Rev. Microbiol. 5:230-239.
13. Hunter GAM, Guevara Vasquez F, Keener JP (2013) A mathematical model and quantitative comparison of the small RNA circuit in the *Vibrio harveyi* and *Vibrio cholerae* quorum sensing systems. Phys. Biol. 10:046007.
14. Jung SA, Hawver LA, Ng WL (2016) Parallel quorum sensing signaling pathways in Vibrio cholerae. Current genetics 62(2):255-260.
15. Lenz DDH, Mok KC, Lilley BN, Kulkarni RV, Wingreen NS, Bassler BL (2004) The small RNA chaperone Hfq and multiple small RNAs control quorum sensing in *Vibrio harveyi* and *Vibrio cholerae*. Cell 118:69-82.
16. Lohmiller W, Slotine JJE (1998) On contraction analysis for non-linear systems. Automatica, 34:683-696.
17. Long T, Tu KC, Wang Y, Mehta P, Ong NP, Bassler BL, Wingreen NS (2009) Quantifying the integration of quorum-sensing signals with single-cell resolution. PLoS Biol. 7(3): e1000068.
18. Miyashiro T, Ruby EG (2012) Shedding light on bioluminescence regulation in Vibrio fischeri. Mol.Microbiol. 84:795-806.
19. Ng WL, Bassler BL (2009) Bacterial quorum-sensing network architectures. Annu. Rev. Genet.43:197-222.
20. Papenfort K, Bassler BL (2016) Quorum sensing signal-response systems in Gram-negative bacteria. Nat. Rev. Microbiol. 1:577-588.
21. Popat R, Cornforth DM, McNally L, Brown SP (2015) Collective sensing and collective responses in quorum-sensing bacteria. J. R. Soc. Interface 12: 20140882.
22. Qian H (2012) Cooperativity in cellular biochemical processes. Annu. Rev. Biophys. 41:179-204.
23. Redfield RJ (2002) Is quorum sensing a side effect of diffusion sensing? Trends Microbiol. 10:365-370.
24. Russo G, Slotine JJE (2010) Global convergence of quorum sensing network. Phys. Rev. E 82:041919.
25. Seger J, Brockman H (1987) What is bet-hedging? In Oxford Surveys in Evolutionary Biology 4:182-211. Oxford University Press, Cambridge, UK.
26. Swem LR, Swem DL, Wingreen NS, Bassler BL (2008) Deducing receptor signaling parameters from in vivo analysis: LuxN/AI-1 quorum sensing in *Vibrio harveyi*. Cell 134:461-473.
27. Teng SW, Schaffer JN, Tu KC, Mehta P, Lu W, Ong NP, Bassler BL, Wingreen NS (2011) Active regulation of receptor ratios controls integration of quorum-sensing signals in Vibrio harveyi. Mol. Syst Biol.7:491.

28. Tu KC, Long T, Svenningsen SL , Wingreen NS, Bassler BL (2010) Negative Feedback Loops Involving Small Regulatory RNAs Precisely Control the Vibrio harveyi Quorum-Sensing Response. Molecular Cell 37:567-579.
29. Wei Y, Ng WL, Cong J, Bassler BL (2012) Ligand and antagonist driven regulation of the *Vibrio cholerae* quorum-sensing receptor. CqsS. Mol. Microbiol. 83:1095-1108.
30. West SA, Winzer K, Gardner A, Diggle SP (2012) Quorum sensing and the confusion about diffusion. Trends Microbiol. 20:586-594.
31. Williams JW, Cui X, Levchenko A, Stevens AM (2008) Robust and sensitive control of a quorum sensing circuit by two interlocked feedback loops. Molecular systems biology, 4:.234.
32. Zhu J, Chai Y, Zhong Z, Li S, Winans SC (2003). Agrobacterium bioassay strain for ultrasensitive detection of N-acylhomoserine lactone-type quorum-sensing molecules: detection of autoinducers in Mesorhizobium huakuii. Applied and Environmental Microbiology, 69(11):6949-6953.